2023 IEEE/ASME International Conference on Advanced Intelligent Mechatronics (AIM)
June 28-30, 2023. Seattle, Washington, USA

Dynamics Analysis and Simulation of an Open-Chain Tetrahedral Robot*

Yubin Wang, Zhenjun Shen, Qian Yang, Yichen Bao and Dongdong Chen

Abstract— **Tetrahedral robots have broad application prospects in the field of space exploration, showing the advantages of high adaptability to the environment and controllable motion trajectory. An open-chain tetrahedral robot is proposed in this paper. Based on the motion form of the robot, its equivalent plane mechanism is established and the kinematic model of the robot is derived. The dynamics of it in its deformation phase is modeled by using the Lagrangian formulation to solve for the required torques of its drive joints. The model was solved and analyzed, and the calculated outcomes were compared with the simulation results in ADAMS. The average relative errors between them did not exceed 10%, which mutually verified the correctness of the theoretical and simulation models. The causes of the data errors are analyzed, providing an essential theoretical basis for the subsequent structural optimization and gait design of the robot.**

I. Introduction

Mobile robots are often used to perform activities in hazardous environments and to do tasks or missions that humans cannot do. Traditional mobile robots cannot handle complex ground environments while tumbling robots have significant advantage in deep space exploration missions[1]. Due to the motion form that brings no fear of tipping in facing unknown terrains and climates, tumbling robots have good development prospects.

The tetrahedral tumbling robot is the simplest structural form of a tumbling robot, originally proposed by Curtis et al. in 2004 [2]. It is a truss structure consisting of six connecting rods and four nodes, which corresponds to the prongs and vertices of an orthotetrahedron, respectively. The robot's center of gravity is shifted by the telescoping of the rods which connects the nodes to produce a tumbling motion [3-5]. On this basis, tumbling robots in the form of octahedra or multiple tetrahedra formed by combining multiple tetrahedral units have been designed and analyzed one after another [6-10]. In addition, the tumbling robot designed by Wang et al. eliminated the telescopic structure of the connecting rod and added a rotating joint in the middle of the connecting rod to deform the robot [11, 12].

For tumbling robots, whether driving joints' output can meet the needs of the robot's deformation requirements is the key to the robot's moving. There are few studies discuss the output forces required for telescoping joints in relevant tetrahedral robots. Li analyzed and optimized the joint torques for their tetrahedral robot with revolute joints[12].

*Research supported by the financial sponsorship from the Shanghai Sailing Program (Grant No. 22YF1412800).

Y. Wang, Z. Shen, Q. Yang, Y. Bao and D. Chen are with the School of Mechatronic Engineering and Automation, Shanghai University, Shanghai, China (corresponding author: Dongdong Chen. E-mail: winterchen@shu.edu.cn).

The current structure of the tetrahedral robot is mainly a deformable truss. Its form determines that at each vertex, there are three kinematic chains converge. This causes the motion branches of the robot to be correlated with each other, posing design and analysis difficulties. The analysis and research on tetrahedral robots are therefore mainly focused on kinematic models and the corresponding simulation analysis, while there is a lack of research related to the drive capability of the drive unit. Because of these characteristics of the existing tetrahedral robots, this paper proposes an open-chain tetrahedral robot, which has the advantages of a simpler structure and lower difficulty in planning the motion process compared with the corresponding truss-type structure. On this basis, the drive capability of its drive joints is analyzed to provide a theoretical basis for the structural optimization design and motion design of the robot.

II. Mechanical and Motion Design

A. Mechanical design

Fig. 1 shows the mechanical structure of the open-chain tetrahedral robot, which consists of four legs having the same structure called Legs A, B, C and D. Each leg of the robot is connected to the central block M by a revolute joint that makes it swing. A passive roller is set at the end of the leg to reduce the friction in a particular direction. Take Leg D as an example, the swing joint is driven by a motor with a controller that allows the leg to swing as required. The swing direction of it is adjusted by a corresponding motor inside the central block. In Fig. 1, the robot is in its initial state. Its four legs' extensions converge at the center of the robot, and the axis of the four swing joints parallel to the ground. In addition, the swing plane of leg D is adjusted to overlap with the swing plane of leg A. In the initial state, due to the symmetry of the robot, the robot forms an orthotetrahedron, and the endpoints of the four legs are located on the four corresponding vertices of the orthotetrahedron.

B. Motion design

The robot relies on its deformation to move the COG (center of gravity) out of the support area and tumble. The specific deform method is: (1) select two legs on the ground to remain stationary as the support legs during tumbling. (2) The leg in the air adjust its direction to swing towards the endpoints of the two support legs. (3) The remaining support leg on the ground swings inward to lift the robot itself. With the help of the swinging leg in the air, the tumbling behavior will be achieved.

Selecting different support legs and adjusting the swing direction of the leg in the air can make the robot move in different directions. For example, as Fig. 2(a) shows, the robot will tumble around the BC endpoint line under the swinging of Leg A and Leg D, while in Fig. 2(b), the robot will tumble

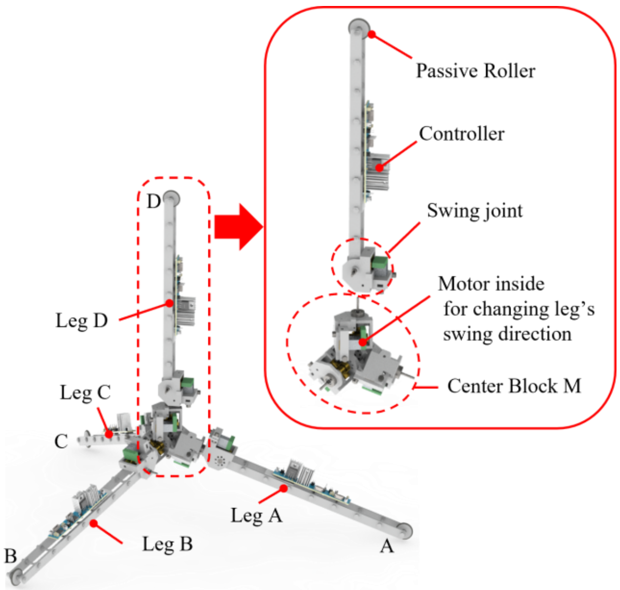

Figure 1. The mechanical structure of the open-chain tetrahedral robot

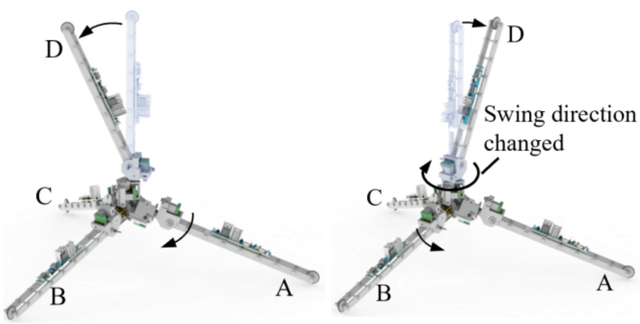

(a) robot will tumble around BC (b) robot will tumble around AC

Figure 2. Different supporting legs for different move directions

around the AC endpoint line under the swinging of Leg B and Leg D.

Taking tumbling around line BC as an example, Fig. 3 shows the moving cycle of the robot with three stages. The first stage is called the deformation stage before tumbling, corresponding to Fig. 3(a) to Fig. 3(b). In this stage, the robot swings Leg A and Leg D to move its COG towards the direction of the line BC. When the robot deforms to the critical position as shown in Fig. 3(b), Leg A and Leg D stop their moving. Under the action of the gravity, the robot will tumble around the line BC as a whole. This is the second stage, called the tumbling stage, corresponding to Fig. 3(b) to Fig. 3(c). The final stage in the movement cycle is called the recovery stage corresponding to Fig. 3(c) to Fig. 3(d). In this stage, the swing angles of Leg A and Leg D, which changed before, are restored, and then the orientation of each leg is adjusted by the center block M, in preparation for the subsequent moving cycle. Since the robot only tumbles as a rigid body by the gravity in the tumbling stage, and the motions of the robot in the recovery stage are only the supporting legs switching. (The motion patterns and dynamics characteristics in the recovery stage are the same as the ones in the first stage.) This paper mainly analyzes the robot in its deformation stage.

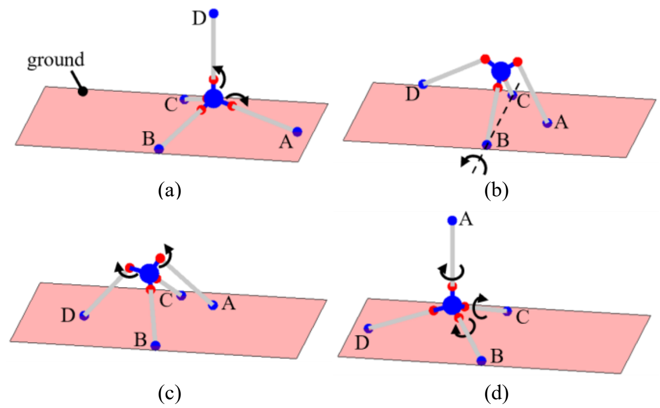

Figure 3. The moving cycle of the robot

III. Kinematics and Dynamics in Deformation Stage

A. Coordinate system and the kinematic model

According to the symmetry structure of the open-chain tetrahedral robot and the fact that Leg B and Leg C remains stationary as the supporting leg during the motion process, the robot always maintains its symmetry in the plane defined by points A, M, and D during the moving cycle. Therefore the robot can be projected to this plane as a equivalent planar mechanism to study its deformation. As shown in Fig. 4, the projection point of point B (also point C), which is the midpoint of line BC, is defined as the origin of the coordinate system, which is denoted as O. Swing joints of the robot are represented by points o_i (i = A, B, C, D) in the mechanism. The coordinate system is established with the OA direction as the x-axis and the vertical ground direction facing upward as the y-axis. In the process of deformation before the robot tumbles, point A as a support point will not be off the ground, so it can be regarded as a slider moving along the x-axis. The lengths from the center M to the swing joints are equal and denoted as r, and the lengths of the swing legs from the joints are represented as l. Let $\angle O_AMO_B$ be α, whose angle is a constant value which is determined by the orthotetrahedral structure in the projection. Let $\angle MOO_A$ be θ_r, and this angle is entirely determined by the robot structure parameters r and l. OO_A is the length of the equivalent connecting rod that actually rotates around O, which is denoted as l_α, and its angle with the positive direction of the x-axis of the coordinate system is designated as θ_1. The swing angles of joints on the corresponding legs are noted as θ_A and θ_D respectively, and the positive directions are defined to facilitate the occurrence of tumbling. The parameters mentioned above are plotted in Fig. 4(a) and Fig. 4(b). In the motion pattern described in Section II, only the swing angles of leg A and leg D joints change during the deformation stage, and these two angles define a specific robot's state. The robot in the deformation stage and its mechanism has two DOFs(degrees of freedom). In this paper, the swinging angles θ_A and θ_D driven by the motor are taken as generalized coordinates for subsequent analysis.

From the definition of the coordinate system and the equivalent plane mechanism, the positions of the two endpoints B and C always stay at the origin while θ_A and θ_D change:

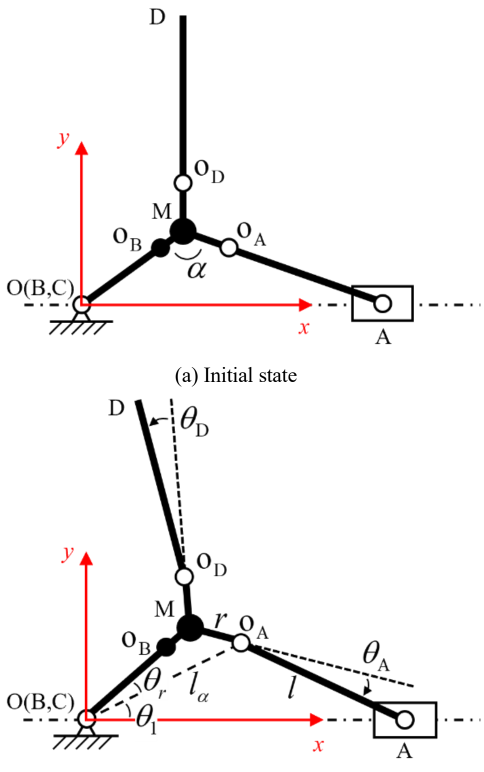

(a) Initial state

(b) Deformation state

Figure 4. Equivalent plane mechanism and coordinate system definition

$$p_{\mathrm{B}} = p_{\mathrm{C}} = \begin{bmatrix} 0 \\ 0 \end{bmatrix} \tag{1}$$

The position of point A and θ_1 can be solved directly from $\triangle \mathrm{OO_A A}$:

$$p_{\mathrm{A}} = \begin{bmatrix} \sqrt{l_\alpha^2 + l^2 - 2l_\alpha l \cos(\alpha + \theta_r - \theta_{\mathrm{A}})} \\ 0 \end{bmatrix} \tag{2}$$

$$\theta_1 = \arcsin\left(\frac{l \sin(\alpha + \theta_r - \theta_{\mathrm{A}})}{\sqrt{l_\alpha^2 + l^2 - 2l_\alpha l \cos(\alpha + \theta_r - \theta_{\mathrm{A}})}} \right) \tag{3}$$

where $l_\alpha = \sqrt{r^2 + 2r(l+r)/3 + (l+r)^2/3}$, and positions of the remaining points of the robot can be solved as:

$$p_{\mathrm{D}} = \begin{bmatrix} \sqrt{l_\alpha^2 + l^2 - 2l_\alpha l \cos(\alpha + \theta_r - \theta_D)} \cos(\theta_1 + 2\theta_r + \theta_2) \\ \sqrt{l_\alpha^2 + l^2 - 2l_\alpha l \cos(\alpha + \theta_r - \theta_D)} \sin(\theta_1 + 2\theta_r + \theta_2) \end{bmatrix} \tag{4}$$

$$p_{\mathrm{M}} = \begin{bmatrix} r' \cos(\theta_1 + \theta_r) \\ r' \sin(\theta_1 + \theta_r) \end{bmatrix} \tag{5}$$

$$p_{\mathrm{oA}} = \begin{bmatrix} l_\alpha \cos\theta_1 \\ l_\alpha \sin\theta_1 \end{bmatrix} \tag{6}$$

$$p_{\mathrm{oB}} = p_{\mathrm{oC}} = \begin{bmatrix} \dfrac{l}{\sqrt{3}} \cos(\theta_1 + \theta_r) \\ \dfrac{l}{\sqrt{3}} \sin(\theta_1 + \theta_r) \end{bmatrix} \tag{7}$$

$$p_{\mathrm{oD}} = \begin{bmatrix} l_\alpha \cos(\theta_1 + 2\theta_r) \\ l_\alpha \sin(\theta_1 + 2\theta_r) \end{bmatrix} \tag{8}$$

where $r' = (r+l)/\sqrt{3}$, $\theta_r = \arcsin(r \sin\alpha / l_\alpha)$, $\alpha = \arccos(-1/\sqrt{3})$,

$$\theta_2 = \arcsin\left(\frac{l \sin(\alpha + \theta_r - \theta_{\mathrm{D}})}{\sqrt{l_\alpha^2 + l^2 - 2l_\alpha l \cos(\alpha + \theta_r - \theta_{\mathrm{D}})}} \right).$$

C. *Dynamics: Joint torque solving*

In the deformation stage, the robot's shape is relied on the motor-driven swing joints on leg A and leg D. Whether the joints' driving torque can meet the robot's deformation needs is an essential condition to determine if the robot can do the tumbling successfully. By the kinematic model, the motion law of each part of the robot with θ_{A} and θ_{D} has been solved. In this section, the dynamics of the robot is established based on the Lagrangian formula. τ_{A} and τ_{D} are solved as:

$$\tau_i = \frac{d}{dt}\left(\frac{\partial \mathcal{L}}{\partial \dot{\theta}_i} \right) - \frac{\partial \mathcal{L}}{\partial \theta_i} \tag{9}$$

where i = A, D, and $\mathcal{L}$ is called the Lagrangian function which is defined as the kinetic energy E_{k} minus the potential energy E_{p} of the whole robot body.

Assume that each leg of the robot has the mass m_i and is uniformly distributed, such that the lengths from swing joints to their center of mass are $l_{\mathrm{c}} = l/2$. The central block M is approximated as a homogeneous ball with a mass of m_{M}. This gives where the center of mass on each component of the robot:

$$p_{\mathrm{Mc}} = p_{\mathrm{M}} \tag{10}$$

$$p_{ic} = \frac{1}{2}(p_i + p_{oi}) \tag{11}$$

where i = A, B, C, D. From Fig. 4(b), it can be seen that when θ_{D} changes, leg D will rotate around $\mathrm{O_D}$. And when θ_{A} changes, the whole mechanism will rotate around point O, except for the rotation of leg A around $\mathrm{O_A}$. Thus, the overall kinetic energy E_{k} of the robot is:

$$\begin{aligned} E_{\mathrm{k}} &= \frac{1}{2} m_{\mathrm{M}} v_{\mathrm{Mc}}^2 + \frac{1}{2} J_{\mathrm{M}} \omega_{\mathrm{Mc}}^2 + \sum_i \left(\frac{1}{2} m_i v_{ic}^2 + \frac{1}{2} J_i \omega_{ic}^2 \right) \\ &= \frac{1}{2}\left(m_{\mathrm{M}} p_{\mathrm{M}}^{\mathrm{T}} p_{\mathrm{M}} + m_i \sum_i p_{ic}^{\mathrm{T}} p_{ic} \right) \dot{\theta}_1^2 + \\ &\quad \frac{1}{2}(J_{\mathrm{M}} + 2J_i)\dot{\theta}_1^2 + \frac{1}{2} J_i \dot{\theta}_{\mathrm{A}}^2 + \frac{1}{2} J_i \dot{\theta}_{\mathrm{D}}^2 \end{aligned} \tag{12}$$

where i = A, B, C, D. In (12), $J_{\mathrm{M}} = 2m_{\mathrm{M}} r^2/5$ is the rotational inertia of the homogeneous ball around its center and $J_i = m_i l^2/12$ is the rotational inertia of the homogeneous rod around its axis through the center. Taking the zero potential energy location at $y = 0$, the potential energy E_{p} of the robot is:

$$E_{\mathrm{p}} = m_{\mathrm{M}} g y_{\mathrm{Mc}} + \sum_i m_i g y_{ic} \tag{13}$$

where i = A, B, C, D. In (13), g is the gravitational acceleration, y_* represents the vertical coordinate of its corresponding position p_*. The generalized forces $\tau_A(t)$ and $\tau_D(t)$, which are determined by the generalized coordinates $\theta_A(t)$ and $\theta_D(t)$ when the robot deforms on the ground, can be calculated by combining (9) ~ (13), and they are the torque requirements for the robots moving.

IV. Simulations in the Deformation State

A. Simulation model building

In order to verify the correctness of the robot's dynamics, a simplified model for simulation was built in ADAMS for experiments. The simplified robot model is shown in Fig. 5. In the model, the ball in the middle represents the center block M. The four legs are represented using connecting rods, and each leg is connected to the central block by using a revolute pair. The mass of each component is uniformly distributed. Contact constraints are added between the robot's legs and the ground. During the deformation stage, the friction between Leg A and the ground is greatly reduced compared to Legs B and C, due to the rollers at the end of Leg A. Therefore, in the simulation model, the friction coefficient between leg A and the ground is set to 0. At the simulation beginning, the robot is placed in its initial state. The dimensional and mass parameters of the model are listed in TABLE I.

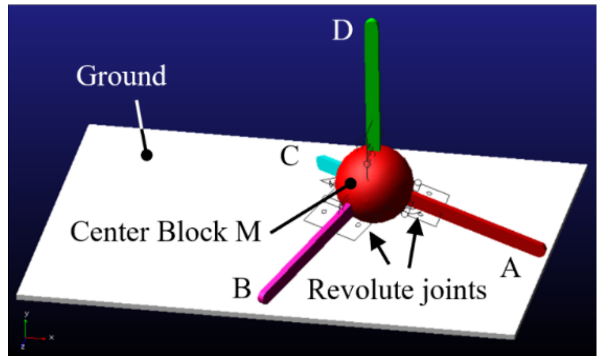

Figure 5. Simplified robot model for simulation

TABLE I. Parameters of the Model

Parameter	Value
Radius of central block r	70 mm
Length of each leg l	244 mm
Mass of central block m_M	0.372 kg
Mass of each leg m_i	0.048 kg
Gravitational acceleration g	9.8 m·s^{-2}

B. Simulation results and their analysis

The simulation time was set to 0~2 seconds, and the number of steps was set to 10000. Three experiments according to different motion rules were conducted under this condition to obtain the curves for τ_A and τ_D. After removing the abnormal data points which are obvious violent jitters in the ADAMS outputs, the results are shown in Fig. 6-8 respectively.

Their corresponding subplots (a) show the rules of motion of θ_A and θ_D for the experiments, and subplots (b) show the patterns of the torque required to drive the swing joints. The simulation data were obtained by ADAMS and the analyzed ones were from the dynamics model listed in (9) ~ (13). The relative errors were plotted in subplots (c). Errors were calculated as $\left|value_{simulated} - value_{calculated}\right| / value_{simulated}$.

Fig. 6 shows the situation when the robot changes θ_A only. In the first second, τ_A gradually decreases and τ_D gradually increases from 0 during θ_A changes to a large value. When θ_A becomes larger, the robot lifts itself up as shown in Fig. 3(b). Leg D changes from vertically upward to inclined outward, and in order to keep θ_D at 0, the swing joint on Leg D also needs to provide a torque to against the influence of the gravitational moment on Leg D. The positive value of τ_A in Fig. 6(b) indicates that the output torque direction is in consistent with the angle direction of θ_A defined in Fig. 4. And the negative value of τ_D indicates that its output torque is opposite to the angle direction of θ_D. The torque directions are all consistent with their expected behaviors. The reason for the gradual decrease of τ_A in the period of second 0 to second 1 is that in this process, the robot's over COG is shifting towards to the line made of point B and C, which reduces the force between point A and the ground. Additionally, the increasing angle between Leg A and the ground during the process also reduces the force arm of the supporting force on the joint. That τ_D in Fig. 6(b) in the period of second 0 to second 1 keeps getting larger is due to the fact that the skew of the robot as a whole gets larger during this period, and for the swinging joint on Leg D, in order to maintain the posture of Leg D, the joint must output a greater torque to counteract the increased torque of gravity on Leg D. The processes during 1 to 2 seconds are opposite to the above, and the images of the moments in Fig. 6(b) are also symmetrical to those in the first second. As can be seen from Fig. 6(c), the relative errors of the two moments also reaches the maximum value in the whole process at the time of 1 second (It is when θ_A reaches its maximum). The reason for this discrepancy is that the deformation can alter the point of contact between Leg A and the ground in the simplified 3D model used for simulation, resulting in a length error within the model and affect the torque output. Most of the relative errors are within 15%, except for the large values of the relative errors caused by the theoretical values of τ_D are very close to 0 at the beginning and the end moments.

Fig. 7 shows the situation when the robot changes only θ_D. As Leg D is not a supporting leg, its movement solely affects the mass moving of Leg D when it swings. It can be seen that when θ_D becomes larger, the overall center of gravity of the robot moves a small distance in the negative x-axis direction, which makes the force between Leg A and the ground decrease. Thus, τ_A decrease. When θ_D is 0, Leg D is theoretically vertical, the gravity of itself passes through the rotation joint, and the required driving moment is 0. As θ_D gets increases, the gravitational moment exerted on the swing joint of Leg D also increases, leading to a greater required moment to maintain the posture. Since there is no movement of the support Leg A, there is no length error caused by the 3D model contact points changing. It can be seen that the torque errors shown in Fig. 7(c) in this case are small, and most relative errors are within 5%.

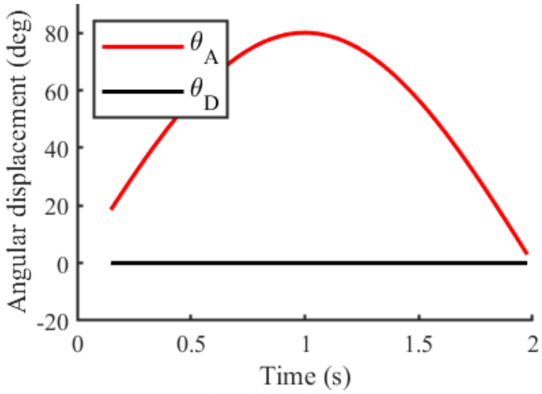

(a) θ_A and θ_D with time

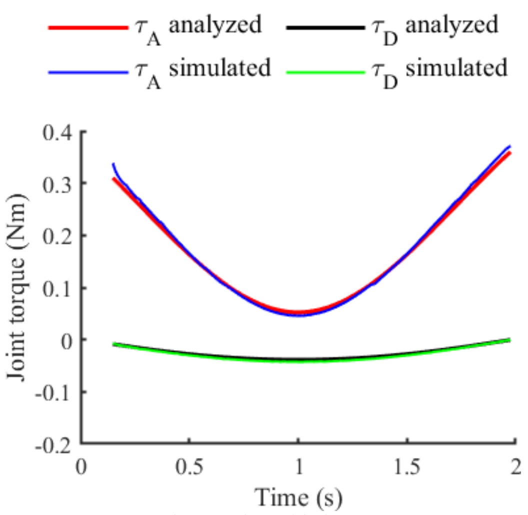

(b) τ_A and τ_D with time

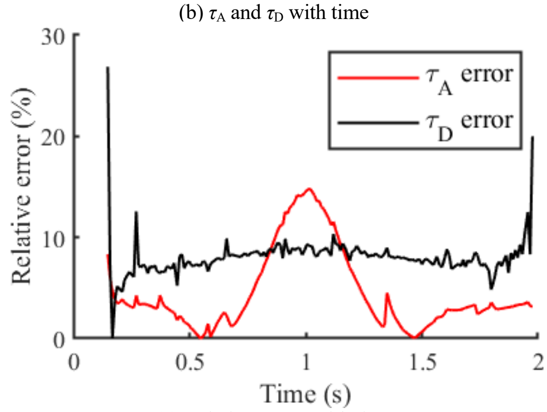

(c) Relative errors with time

Figure 6. Robot changes θ_A only

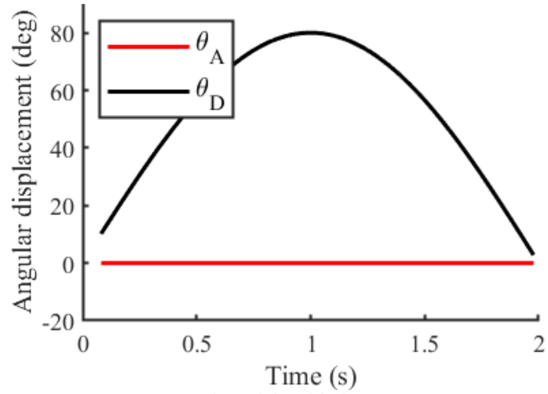

(a) θ_A and θ_D with time

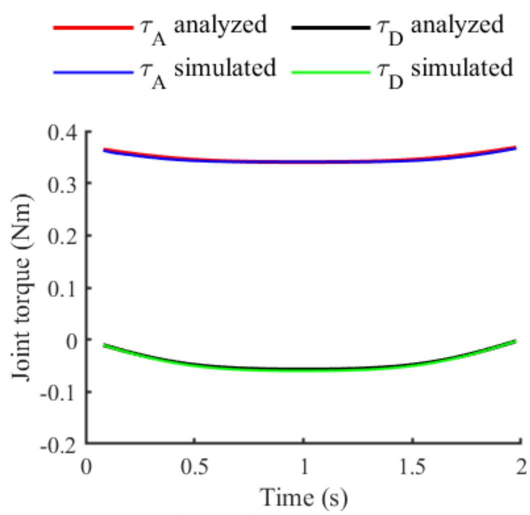

(b) τ_A and τ_D with time

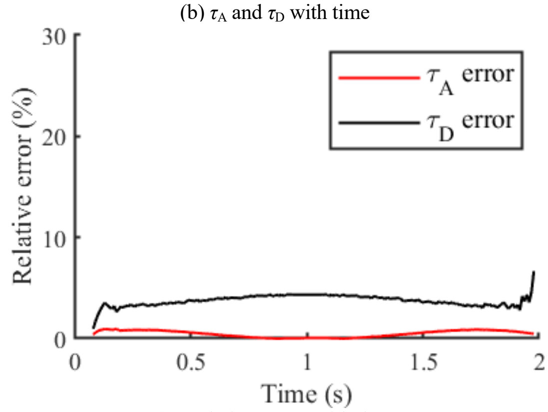

(c) Relative errors with time

Figure 7. Robot changes θ_D only

Fig. 8 shows the situation for θ_A and θ_D changes simultaneously in a complex way. From Fig. 8(b), it can be seen that the results obtained from simulation and calculation are in good agreement. The maximum absolute error of τ_A in the figure occurs at the beginning of it, which is 0.0218Nm, and the maximum absolute error of τ_D curve occurs at t = 0.2918, which is only 0.0064Nm. The relative error curves are shown in Fig. 8(c), where the relative error is large when τ_D is near 0. Otherwise, the relative errors are mostly within 15%.

From Figs. 6-8, we can see that the dynamic model obtained in this paper is consistent with the results from the ADAMS simulation, and the average relative errors of the three experiments are shown in TABLE II. The average relative errors in these three situations are within 10%, which demonstrates that the simulations and calculations carried out in the article mutually confirm each other's accuracy and reliability[13]. The relative errors are the smallest when the robot act θ_D only. That is because θ_A keeps unchanged will not cause supporting point in Leg A to move, which relates to the length error of OO_A. The relative errors of θ_D are larger than θ_A in all the three cases. It is because the theoretical values of τ_D are close to 0, but the τ_A. The curves in Figs. 6-8 show that the analyzed joint torques are all close to simulated ones, which means that the absolute errors are small.

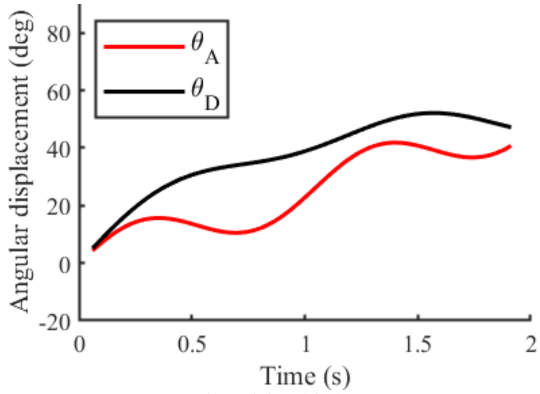

(a) θ_A and θ_D with time

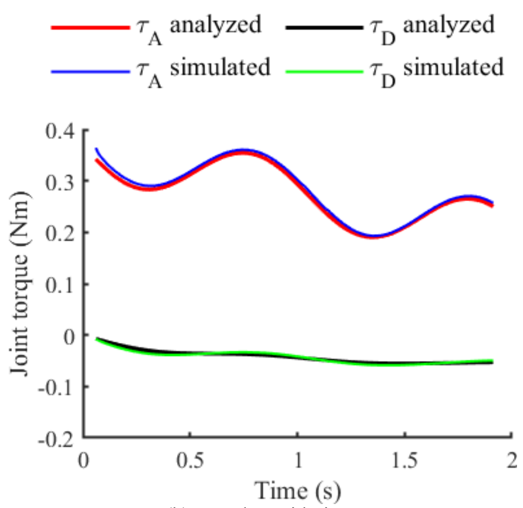

(b) τ_A and τ_D with time

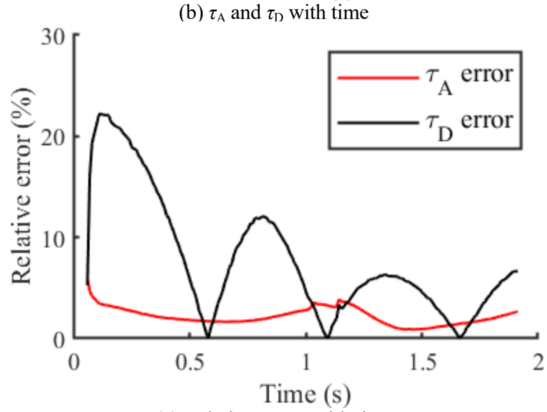

(c) Relative errors with time

Figure 8. Robot changes θ_A and θ_D in complex rules

TABLE II. AVERAGE RELATIVE ERRORS

Situation	Error of τ_A	Error of τ_D
θ_A changes only	4.59 %	8.05 %
θ_D changes only	0.47 %	3.74 %
θ_A and θ_D change together	2.17 %	7.67 %

V. CONCLUSION

In conclusion, an open-chain tetrahedral robot is proposed in this paper. The structure, moving mode and its equivalent planar mechanism were introduced and discussed. The dynamics of the robot was derived from the Lagrangian formulation, and the required driving torques for deformation were calculated. By comparing with the outcomes simulated by ADAMS, the correctness of the analyses got mutually verified with the average torque errors being less than 10%. It was analyzed that the errors mainly came from the simplified 3D modeling, where an equivalent length will be changed by the contact point moving in the simulation process. In general, the results of the two calculation methods were in agreement, which reflected that the planar mechanism of the robot plays a good role in the open-chain tetrahedral robot analysis. In the future, the work consumed by joints during robot's motion based on the driving torques will be analyzed, which will be helpful for the robot's gait design. The robot's gait utilizing inertial forces for rolling will be studied, allowing the robot to move in complex ground environments.

ACKNOWLEDGMENT

The authors are grateful to the financial sponsorship from the Shanghai Sailing Program (Grant No. 22YF1412800).

REFERENCES

[1] S. Curtis *et al.*, "TET Rovers: An Approach for Exploring Rugged Terrains with Addressable Reconfigurable Technology," in *37th Annual Lunar and Planetary Science Conference*, Houston, 2006, pp. 1129.

[2] S. Curtis *et al.*, "Tetrahedral Robotics for Space Exploration," *IEEE Aerospace and Electronic Systems Magazine*, vol. 22, no. 6, pp. 22–30, Jun. 2007.

[3] M. Abrahantes, P. Doorn, J. Richard, and S. Barbachyn, "Implementation and control of a reconfigureable 4-tetrahedral robot," in *2009 41st Southeastern Symposium on System Theory*, Tullahoma, 2009, pp. 344-349.

[4] M. Izadi, M. J. Mahjoob, M. Soheilypour, and H. Vahid-Alizadeh, "A Motion Planning for toppling-motion of a TET Walker," in *2010 The 2nd International Conference on Computer and Automation Engineering*, Singapore, 2010, pp. 34-39.

[5] L. Zhang, S. Bi, and Y. Cai, "Design and Motion Analysis of Tetrahedral Rolling Robot," in *2010 IEEE/RSJ International Conference on Intelligent Robots and Systems*, Taipei, 2010, pp.502-507.

[6] M. Abrahantes and C. Smits, "Implementation and Control of a Reconfigurable 8-Tetrahedral Robot," in *2012 IEEE International Conference on Electro/Information Technology,* Indianapolis, 2012, pp. 1-5.

[7] M. Abrahantes, A. Silver, and L. Wendt, "Gait Design and Modeling of a 12-Tetrahedron Walker Robot," in *2007 Thirty-Ninth Southeastern Symposium on System Theory*, Macon, 2007, pp. 21-25.

[8] X. Wang, X. Wang, Z. Zhang, and Y. Zhao, "Motion Planning of Kinematically Redundant 12-tetrahedral Rolling Robot," *International Journal of Advanced Robotic Systems*, vol. 13, no. 1, pp. 23, Jan. 2016.

[9] R. Liu, Y. Yao, and Y. Li, "Design and Analysis of a Deployable tetrahedron-based Mobile Robot Constructed by Sarrus Linkages," *Mechanism and Machine Theory*, vol. 152, pp. 103964, Oct. 2020.

[10] W. Ding, S.-C. Kim, and Y.-A. Yao, "A Pneumatic Cylinder Driving Polyhedron Mobile Mechanism," *Frontiers of Mechanical Engineering*, vol. 7, no. 1, pp. 55–65, Mar. 2012.

[11] Z. Wang, Y. Tian, and Y. Yao, "A Novel Underactuated Tetrahedral Mobile Robot," *Journal of Mechanisms and Robotics*, vol. 10, no. 4, Jun. 2018.

[12] Y. Li, Z. Wang, Y. Xu, J. S. Dai, Z. Zhao, and Y. Yao, "A Deformable Tetrahedron Rolling Mechanism (DTRM) Based on URU Branch," *Mechanism and Machine Theory*, vol. 153, pp. 104000, Nov. 2020.

[13] Z. Wang, "Systematic Design and Research on Linkage-based Tetrahedral Mobile Robot," Ph.D. dissertation, Dept. Mech. Eng., Beijing JT Univ., Beijing, China, 2019.